Search for superstrong magnetic fields in active processes on the Sun using spectro-polarimetry within 15 angstroms around the D3 line

I.I. Yakovkin, V.G. Lozitsky[*]

*Astronomical Observatory of the Taras Shevchenko National University of Kyiv,
Kyiv 04053, Ukraine*

ABSTRACT

We critically review our previous results on this topic based on the following main points: (i) substantially larger wavelength range around the D3 line was investigated - up to ±15 Å instead of ±2.5 Å in comparison with the previous version of our study, and (ii) greater volume of observational data was analyzed, including one X limb flare, additionally. Overall, our study concerns the 2004 July 12 active prominence and the 2014 June 10 limb flare of X1.5 class. For named limb flare, we found reliable and oppositely polarized secondary peaks of the V parameter located at distances of -4.5 Å and +2.7 Å from the line center. If these features are interpreted as manifestations of the magnetic splitting of the line together with its Doppler shift, then the corresponding magnetic field is $\approx 2.2 \times 10^5$ G, and the radial velocity -46 km s^{-1}. Similar spectral manifestations were also found in the active prominence. For comparison with the theory, the spectral features of the Paschen-Back effect at magnetic fields up to 100 kG were studied too. It turned out that the theoretical width of the splitting components is relatively small, 0.3 Å, while the width of the observed peaks is sometimes much larger. On the basis of model calculations, it is shown that in some cases an alternative explanation of the observational data is possible, which includes much weaker magnetic fields (5.5-7.1 kG), but significant macroscopic velocities of different signs, at the level of 50-60 km s^{-1}.

Key words: magnetic fields, Sun: activity, Sun: flares, Sun: magnetic fields, Sun: filaments, prominences.

1 INTRODUCTION

Currently, the dominant view is that the strongest magnetic fields on the Sun are observed in sunspots, where their magnitude is typically 2000-3000 G and very rarely - 4000-6000 G (Solanki, 2003; Livingston et al., 2006; Wang et al., 2018; Lozitsky et al., 2022). In spatially unresolved (sub-telescopic) areas of sunspots with a small filling factor, the magnetic fields with a strength of 7-8 kG were found (Van Noort et al., 2013; Lozitsky, 2017). Such magnetic fields were recorded even with a filling factor close to unity (Durán et al., 2020).

For the first time, extremely strong magnetic fields in sunspots with an intensity of more than 10 kG were suspected, apparently, by Severny (1957). He assumed the existence of magnetic fields with a magnitude of 50 kG, but did not provide detailed observational data that would confirm this hypothesis. A set of arguments regarding the existence of specified superstrong fields in sunspots was recently presented in paper by Lozitsky et al. (2022).

[*]E-mail: vsevolod.lozitsky@knu.ua or lozitsky_v@ukr.net

Bruce (1966) was apparently the first who suggested the existence of giant magnetic fields in the range of 10-100 kG in the solar flares. He supposed that long wings of the Hα line in some solar flares, up to 8 Å, can be an indication of such super-strong fields. Since this assumption was based on observations in unpolarized light (Stokes I parameter), it needs additional confirmation. After all, the magnetic field should not only broaden or split the spectral lines due to the Zeeman effect, but also polarize the splitting components accordingly.

Observational data on polarization effects in the emission profiles of spectral lines observed in solar flares are very valuable for elucidating the true magnetic field magnitude directly in the region of significant flare energy release. As for measurements by Frauhofer profiles, they provide information about the magnetic field at the photosphere level, that is, mainly under the solar flare. The magnetic fields in the solar flares, measured by different authors from analysis of the emission manifestations of the Zeeman effect, as a rule, did not exceed typical values for sunspots (see, e.g., Harvey, 2012; Kirichek et al., 2013; Klient, 2017; Libbrecht et al., 2019). However, all such measurements were made in the weak-field Zeeman-splitting approximation (see, e.g., Jefferies and Mickey, 1991; Cauzzi et al., 1993) and can only be considered as the lower estimate of the true field magnitude. The real magnitude of the magnetic field can only be determined in the strong magnetic field mode, when the splitting of the Zeeman sigma components exceeds their own spectral width. This mode can be observed usually in big sunspots using narrow (~ 0.1 Å) magnetically sensitive lines with large Lande factor (g = 2.5-3). It is also important that in sunspots the filling factor is close to one, which provides a very well visible and contrasting picture of the Zeeman splitting.

The emission manifestations of the Zeeman effect in solar flares are usually observed in spectrally broad emissions (≥ 0.5-1 Å), especially in hydrogen and helium lines. In addition, the Lande factors of such lines is low, close to unity. It is these lines that are important for conclusions about the magnetic field in the chromosphere and the transition zone. Narrower emissive manifestations of the Zeeman effect in flares can be observed in the lines of metals, in particular Fe I, but such lines are formed below - in the upper photosphere and the temperature minimum zone (see, e.g., Lozitsky et al., 2000).

Valuable data on magnetic fields in the lower corona can be obtained from observations of limb solar flares. Such observations allow to measure the height in atmosphere directly, without line formation modelling which depends on the flare model which can be very different in various flares. A broad comparison of the results of different authors and methods for solar corona is presented in the paper by Sasikumar Raja et al. (2022). The authors note that the measured magnetic field strength, as whole, increases from ~1 G at 2 solar radii to more than 3 kG at 10-20 Mm (Yakovkin et al., 2021). Magnetic fields in the range of 600-1400 G were also found by Wei Yudian et al (2021) in the partially erupting filament in a solar flare. So long these data were obtained in the weak-field approximation and represent the longitudinal component B_{LOS}, the magnitude of the field strength modulus of local magnetic fields should be actually even greater.

In order to estimate the local magnetic field in the case of a small filling factor, the search for weak spectral manifestations of complete Zeeman splitting is of particular interest. In our

previous paper – Yakovkin & Lozitsky (2022) – we found such manifestations at the distant wings of the Hα line observed in the limb solar flare of July 14, 2005. It has been argued that such spectral manifestations, likely, indicate superstrong magnetic field of ~90 kG in this flare. Possible existence of such fields follows from recently published theoretical work by Solov'ev (2022), in which a new class of force-free solutions for a horizontal magnetic thread with a circular cross-section was considered. It was concluded that the magnetic field intensity on the axis of such configuration is significantly (up to 2–3 orders of magnitude and more) exceeds the intensity of the longitudinal external field that keeps the rope from lateral stretching. That is, it means that if the external magnetic field in the corona is quite weak, then on the axis of the corresponding structures it can be several orders of magnitude higher and possibly reach the very large values indicated above. Of course, this theoretical prediction requires careful testing based on the analysis of observational data. Undoubtedly, the possible existence of such super-strong magnetic fields is currently a "hot" problem in heliophysics.

In this regard, new studies aimed at finding and investigating fine spectral effects that may indicate the super-strong magnetic fields are in high demand. Compared to the previously published article by Yakovkin and Lozitsky (2022), here we analyse (a) substantially larger distances from line center, namely ±15 Å instead of ±2.5 Å (b) a different spectral line, D3 instead H-alpha, and (c) another active processes, which include one X flare and one active prominence.

2 OBSERVATIONS AND DATA PROCESSING

Observations under study (Table 1) were carried out with the Echelle spectrograph of the horizontal solar telescope of the Astronomical Observatory of Taras Shevchenko National University of Kyiv (Lozitsky, 2017). Observers were Natalia Lozitska and Vsevolod Lozitsky for the active prominence and V.L. – for the limb flare.

Table 1 – Some parameters of objects under study and circumstances of observations

Object	Date	Related active region	Peak of X ray, UT	Time of exposure, UT
Active prominence	July 12, 2004	NOAA 10647	08^h15^m	$08^h48^m50^s + 60^s$
X1.5 limb flare	June 10, 2014	NOAA 2087	12^h52^m	$13^h08^m40^s + 20^s$

The main value of observations with the Echelle spectrograph is that a wide spectrum interval, from 3800 to 6600 Å, can be recorded simultaneously where many thousands of spectral lines can be observed. Another advantage of such observations is that $I + V$ and $I - V$ spectra were obtained simultaneously, on separate adjacent bands of the spectrograms. This was made thanks to the fact that the circular polarization analyzer consisted of a λ/4 plate in front of the entrance slit of the spectrograph and a beam splitting prism (analogous to the Wollaston prism) behind the entrance slit. Therefore, $I + V$ and $I - V$ spectra relate to the same moment of time and to the same locations on the Sun.

The Echelle spectrograph is a cross-dispersion instrument. Its optical design simultaneously employs a diffraction grating with profiled grooves to intensify light concentration, as well as a

glass prism for dispersing diffraction orders. Therefore, the overlay of diffraction orders is entirely prevented, specifically due to the glass prism dispersing these orders to an appropriate degree. Additional details about our telescope and spectrograph can be found in the publication by Lozitsky (2016).

The D3 line was observed by this instrument in the 35th order of diffraction, and the total length of the spectrum, which is simultaneously registered near this line, is 160 Å in the range from -112 Å to +48 Å relative to the center of the D3 line. Dispersion in this order is 770 mÅ per mm, and the full width at half maximum (FWHM) of the instrumental profile is about 50 mÅ. All spectra were photographed on ORWO WP3 photographic plates, which give a signal-to-noise ratio of about 100 when optimally exposed. The length of the entrance slit of the spectrograph was 2.2 mm, and its width was 0.06 mm, which corresponds to about 33 and 0.9 arcsec, respectively. However, due to image vibration, the actual spatial resolution of our observations is ≈ 1.5 Mm.

Positive images of D3 line in spectra of active prominence are presented in Fig. 1. As can be seen from this Figure, the photosphere did not hit the entrance slit of the spectrograph during the observations of the prominence, which does not allow to the reliably link the data to the altitude scale in the solar atmosphere. Taking into account this circumstance, we can only indicate approximate heights in the atmosphere, based on sketches of the edge of the solar disk relative to the entrance slit of the spectrograph. The prominence heights indicated in Fig. 1 represent the lower limit of the actual heights, and the actual heights may be about 5 Mm higher than those specified.

From Fig.1 it follows that the appearance of the D3 line in the spectrum is relatively simple, typical for arched structures, in which there are significant differences in radial velocities in the "legs" of the arch and close to zero velocities at its top. Of course, in this case, it is more correct to speak not about a separate arch, but a certain collection of small-scale spatially unresolved arches (arcade), averaged by our instrument due to its limited spatial resolution (~ 1.5 Mm).
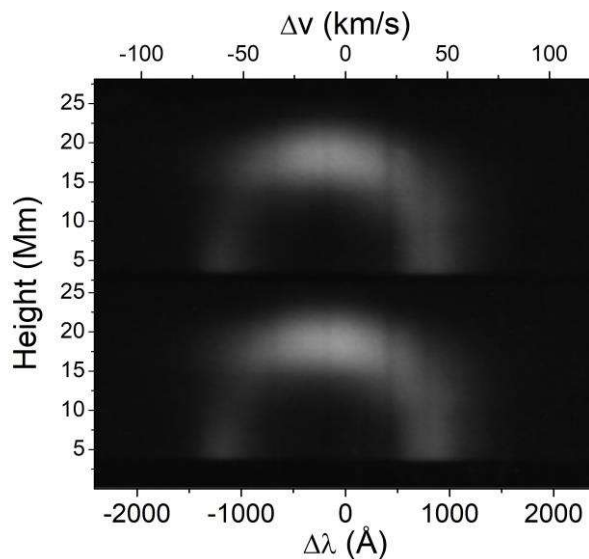

Figure 1. Fragments of the Zeeman spectrogram which show the D3 He I line in active prominence of July 12, 2004. The top and bottom half of spectrograms correspond to the $I - V$ and $I + V$ spectra, respectively. The zero-point on the abscissa corresponds to $\lambda = 5875.6$ Å (Moore et al., 1966).

As can be seen from the Figure, the difference in speeds in the "legs" of the arcade reaches 100 km s^{-1}, and at the top of the arcades the absolute value of the speed is relatively small, about -25 km s^{-1} (the minus sign means the movement of the plasma in the direction of the observer). Since the emission in D3 is more intense at the top of the arcades, it is apparent that an almost longitudinal magnetic field can be expected at the top of the arcades, when the angle between the line of sight and the direction of the field lines is close to zero. Given that our observational data were obtained with a circular polarization analyzer and are suitable for diagnosing the longitudinal Zeeman effect, it is clear that we can hope for positive results in terms of finding particularly strong magnetic fields precisely at the top of the arcade, which in our case corresponds to heights in the range of 16-22 Mm.

The June 10, 2014 limb solar flare was associated with NOAA 2087 active region, which appeared in the eastern disk the next day, June 11, 2014. This active region was small in size, but produced three X flares during June 10-11. When photographing the spectrum of this flare, the photosphere was recorded (Fig. 2), thanks to which it is possible to more accurately indicate the height in the atmosphere to which our spectral data relate. It can be seen that the D3 line here also has a rather simple appearance, without a significant broadening of it at high Doppler velocities.
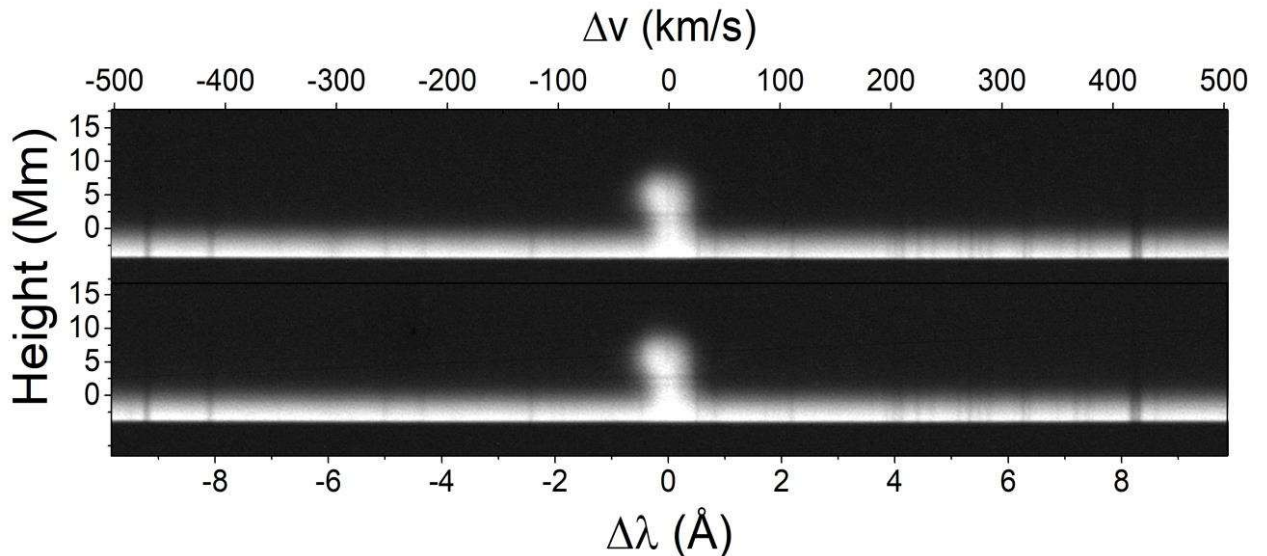
Figure 2. The same as in Fig. 1, but for the solar flare on June 10, 2014.

In order to obtain quantitative information about the D3 line profiles, the spectrogram was scanned using an Epson Perfection V 550 scanner. To transfer blackening into intensity it is necessary take into account the characteristic curve of the photographic material as well as the curve of the scanner itself. Both curves are nonlinear and require preliminary determination by special methods. In order to do this, we used a step attenuator, for which transmittances are precisely known. When converting photometrical densities into intensities, the scattered light in the spectrograph was taken into account by subtracting the intensities corresponding to the

intervals between images of different diffraction orders of the spectrum of the Echelle spectrograph.

During the pre-processing of observational data, spectrum recordings of $I + V$ and $I - V$ profiles in intensities were mutually linked by wavelengths using narrow telluric lines; the accuracy of this binding is about 1-2 mÅ. The next step of data processing was to find the normalized intensities, i.e. local intensities, expressed in units of maximum intensity in the central part of the D3 line profile. Since the absolute intensities of the $I + V$ and $I - V$ spectra differed insignificantly, by about ~ 10% (which is partially seen from Figs. 1 and 2), this normalization led to the fact that the intensities of both spectra leveled off in the central part of the D3, but almost did not change in the distant wings. After these two steps, the I and V profiles were calculated using $I + V$ and $I - V$ profiles.

The spectrum processing procedures were carried out using a custom-developed application. This application significantly streamlines and automates the processing of large quantities of observational data. It offers features such as data smoothing, averaging across multiple photometric sections, and calculating Stokes parameters (including I, V, and $dI/d\lambda$), while also estimating measurement and averaging errors.

Local values of intensities were obtained through scanning with a step of 3.846 mÅ. This extremely fine spectral discretization was used to ensure reliable elimination of very narrow artifacts associated with small dust particles in the spectrogram. These narrowest artifacts, being much narrower than the FWHM of the instrumental profile, were detected and eliminated most effectively at fine discretization. Had a spectral sampling with a step of 50 mÅ been used, it is possible that some artifacts could have been overlooked, potentially introducing significant distortions into the observational data.

In order to search for subtle effects in the spectrum, we found the averaged smoothed intensity profiles by averaging the data over 100 points, i.e., 384.6 mÅ, which is approximately 3 times less than the observed emission width of the D3 line (Fig. 3). If all local measurements were statistically independent, then combining the data for 100 points in the spectrum would increase the signal-to-noise ratio approximately by the factor of 10. However, since the width of the instrument profile of the spectrograph is 50 mÅ, which corresponds to approximately 13 points on a registragram, only those intensity values that are more than the FWHM of the instrument profile can be considered statistically independent. In this case, the real signal-to-noise ratio increased approximately by the square root of 7.7, that is, by the factor of 2.8. In order to reduce the influence of noise effects, we combined photometric data not only by wavelengths in the spectrum, but also by different locations on the Sun, as presented below in the Section 3.

3 DIAGNOSTIC FEATURES OF THE OBSERVED LINE PROFILES

3.1 Active prominence of July 12, 2004

The observed profiles of the D3 line in the prominence (Fig. 3) turned out to be quite symmetrical, despite the fact that this line, theoretically, consists of several closely spaced subcomponents of different intensities (see Sect. 4 below). This is due to the fact that the line D3 $\lambda = 5875.6$ Å belongs to orthohelium and arises when the electron spins in this atom are parallel

(Frish, 2010). The Pauli principle forbids two electrons to be in a state with the same quantum numbers, so electrons in the lower energy state of orthohelium, having the same spins, are forced to have different main quantum numbers: one electron is in the 1S orbital, and the other is in the 2S orbital, which is more distant from the nucleus orbitals (shell state 1S 2S). This gives the triplet structure of this spectral line with distances between the splitting subcomponents in the range of 0.1-0.2 Å. However, when the D3 line is broadened to ≈ 1 Å (as in the case of objects under study), all subcomponents of the line are broadened so much that they form only one profile without significant asymmetry.

The obtained data also have other characteristic features, namely the following:

(1) In the brightest place of the prominence, which corresponds to heights in the range of 18-21 Mm, there is a systematic shift of the $I + V$ profile, shown by a solid line in Fig. 3, relative to the profile $I - V$, which is depicted in the figures with strokes. Such a displacement indicates a certain magnitude of the magnetic field. Assuming that the Lande factor is close to unity for the D3 line, we have the following calibration formula:

$$\Delta\lambda_H = 1.61 \times 10^{-5} B, \tag{1}$$

where the magnetic splitting $\Delta\lambda_H$ is expressed in angstroms (Å), and the magnetic field strength B – in gauss (G).

According calculations using HAZEL code (Asensio Ramos et al., 2008), formula (1) describes well the relationship between $\Delta\lambda_H$ and B in the strength range of 20-100 kG (see section 4 below). However, in the range $B = 500$-2000 G, the calibration formula is slightly different:

$$\Delta\lambda_H = 1.51 \times 10^{-5} B, \tag{2}$$

As can be seen from the comparison of (1) and (2), these two cases give a relatively small difference in the measured magnetic fields, ≈ 6 %.
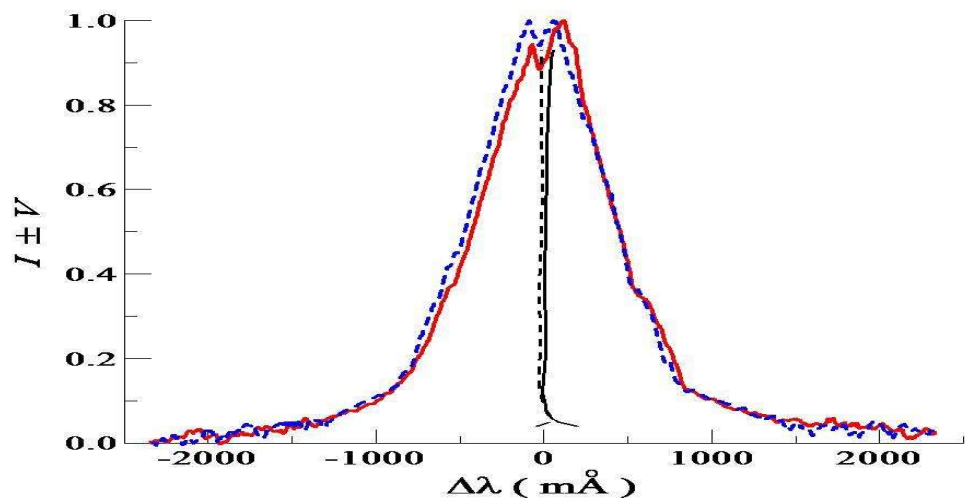
Figure 3. Observed unsmoothed $I \pm V$ profiles of the D3 line in photometric section No. 18, which corresponds to a height of 18 Mm. Almost vertical lines show the bisectors of profiles $I \pm V$.

To measure the relative shift of $I + V$ and $I - V$ profiles, we used the spectral range $\Delta\lambda$ of distances from the line center corresponding to $\Delta\lambda = 200$–400 mÅ, since there is no significant effect of telluric lines on the D3 line profile. The second reason is that the D3 line profiles are the steepest here, giving the highest measurement accuracy.

If we assume that the measured splitting of the bisectors corresponds to $2\Delta\lambda_H$, then the measured magnetic field is in the range of 530-1590 G. Thus, the magnitude of the magnetic field strength in this prominence is approximately the same as according to our measurements in a limb flare using the Hα line (Yakovkin et al., 2021). Notice, the assumption that the measured bisector splitting is equal to twice the Zeeman splitting implies a purely longitudinal magnetic field approximation when the angle γ between the line of sight and the magnetic field line is zero (more precisely, $\gamma = 0°$ or $180°$). If this is not the case, then the true magnetic field should be actually even stronger than the measured value.

(2) It turned out that in the distance interval $\Delta\lambda = 200$–400 mÅ, the value of the measured field intensity B_{meas} changes with the distance $\Delta\lambda$ from the line center: the magnitude of B_{meas} generally increases with decreasing $\Delta\lambda$. This has been repeatedly observed by other authors, in particular Harvey (2012) and Kirichek et al. (2013). This effect indicates the inhomogeneity of the magnetic field: for a uniform magnetic field and weak magnetic splitting (i.e., in the weak field mode, when $\Delta\lambda_H \ll \Delta\lambda_{1/2} = $ FWHM), the measured strengths should be the same for different parts of the profile of spectral line.

Indeed, the weak field mode corresponds to the formula

$$V \sim (\mathrm{d}I/\mathrm{d}\lambda)\Delta\lambda_H . \tag{3}$$

This expression can be obtained from the formula

$$V = 0.5[I(\lambda+\Delta\lambda_H) - I(\lambda-\Delta\lambda_H)], \tag{4}$$

if each of the quantities $I(\lambda+\Delta\lambda_H)$ and $I(\lambda-\Delta\lambda_H)$ is expanded into a Taylor series in powers of $\Delta\lambda_H$ and only the first powers of this parameter are taken for consideration. But from (4) it follows that the profiles $I(\lambda+\Delta\lambda_H)$ and $I(\lambda-\Delta\lambda_H)$ are completely identical to each other, but only shifted relative to each other by $\pm\Delta\lambda_H$. Obviously, this means that the bisectors of the profiles $I(\lambda+\Delta\lambda_H)$ and $I(\lambda-\Delta\lambda_H)$ must be parallel to each other, that is, their splitting corresponds to the same measured magnetic strengths on different distances from line center. If this is not the case, then one of the reasons for this may be the inhomogeneity of the magnetic field in the picture plane (Gordovskyy & Lozitsky, 2014).

(3) The splitting of bisectors seems to increase not only when approaching the emission core of line, but also when moving to its distant wings (Fig. 3). This effect becomes more pronounced if the line profile is averaged by a sliding window 100–400 mÅ wide. However, even in this case, the magnitude of the specified effect approaches the measurement errors for individual photometric sections, given that when averaging the data over 100 points, the real error is reduced not by a factor of 10, but by approximately a factor of 3 (see above, Section 2). In

addition, in the very far wings of the line, where the parameter dI/dλ is very small, the measurement errors grow proportionally to (dI/dλ)$^{-1}$ (Lozitsky, 2015). Therefore, to search subtle spectral effects at large distances from the line center which may indicate particularly strong magnetic fields, it is better to use information about the Stokes V profile rather than bisector splitting.

Given these circumstances, we studied the Stokes V using double averaging of the data: (a) over very wide spectral intervals, around 380 mÅ, which roughly corresponds to 1/3 widths of the intense emission of the D3 line and (b) summarizing five photometric sections corresponding to heights in the interval 16-20 Mm. The result in this regard is presented in Fig. 4 together with the profile of the parameter dI/dλ, which gives the expected form of the parameter V in the approximation of a weak magnetic field.
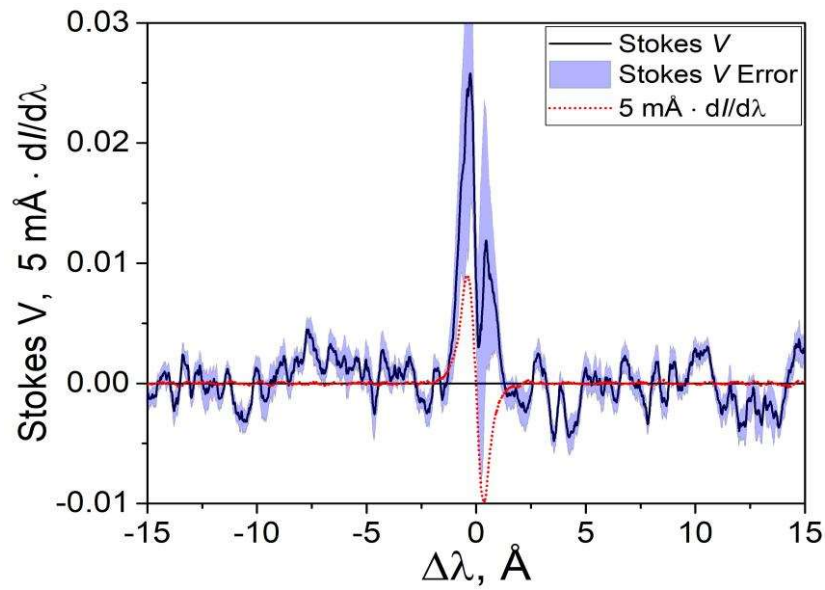
Figure 4. Stokes V profile of the D3 line in the active prominence, averaged over a height interval of 5 Mm. For comparison, the profile of the parameter dI/dλ is shown with a red curve. Shaded area represents the root mean squared error of averaging across the heights of 16 − 20 Mm.

Figure 4 shows that the numerical values of the parameter dI/dλ approach zero at distances $\Delta\lambda$ exceeding 2 Å in absolute value. This means that in the approximation of a weak field at such distances, one cannot expect reliable fluctuations of the parameter V, that is, such fluctuations that exceed the measurement errors. However, it can be seen from the Figure that in the range of distances $|\Delta\lambda| = 2 \div 15$ Å, reliable fluctuations of the parameter V are still observed in some places, and they, at first glance, have an irregular character. A closer look shows that the following interesting feature can be noted: some narrow local peaks are located on both sides of the center of the line at approximately the same distance, almost symmetrically, but with the opposite sign. For instance, a relatively broad negative peak is located at $\Delta\lambda = -10.5$ Å, while a similar-looking positive peak is located at $\Delta\lambda = +10.3$ Å. The situation is similar with a pair of peaks at $\Delta\lambda = -7.7$ Å and $+7.8$ Å. If we assume that these values $|\Delta\lambda| = 7.7$-7.8 Å and 10.3-

10.5 Å correspond to Zeeman splitting, then according to formula (1) the corresponding magnetic fields are 4.81×10^5 G and 6.46×10^5 G, respectively. Observational indications of magnetic fields of similar magnitude were found earlier in a solar flare on the disk, but for the height range of the "upper photosphere - temperature minimum zone", that is, for much denser layers of the solar atmosphere (Lozitsky, 2009). To be sure of the reality of such extremely strong fields, alternative explanations should be considered, which include, for example, the combined effect of Zeeman splitting and high Doppler velocities. This can be done on the basis of simulations, but before this, other observational data should be considered, on the basis of which it is possible to estimate the range of probable changes of the specified parameters.

### 3.2 X1.5 limb flare of June 10, 2014

In this flare, the most intense emission in the D3 line was observed at heights of 3-8 Mm (Fig. 2), and it was in this range that the magnetic fields were studied. It turned out that the splitting of the intense emission peaks of $I \pm V$ profiles correspond to strengths in the range of 400-600 G and S magnetic polarity. Stokes V profile, averaged over the entire height interval of 4-7 Mm, is presented in Fig. 5. It can be seen that the overall picture of the Stokes V has two components: (a) strong and narrow primary peaks localized near the center of the line and having a splitting of about 800 mÅ, and (b) weaker and broad secondary peaks localized mainly in distance intervals of 2-5 Å from the center of the line. As to splitting of $dI/d\lambda$ peaks, it is about 800 mÅ too.

More precisely, the secondary peaks are localized at distances $\Delta\lambda$ = -4.5 Å and +2.7 Å, that is, far beyond the peaks of the $dI/d\lambda$ parameter (Figs. 5 and 6). Given this and the fact that the secondary peaks have the opposite sign of polarization on either side of the center of the line, we can assume a Zeeman effect, but with a significant negative Doppler shift. Under this assumption, the magnitude of the magnetic field and the magnitude of the radial velocity are as follows: 2.24×10^5 G and -46 km s^{-1}, respectively.
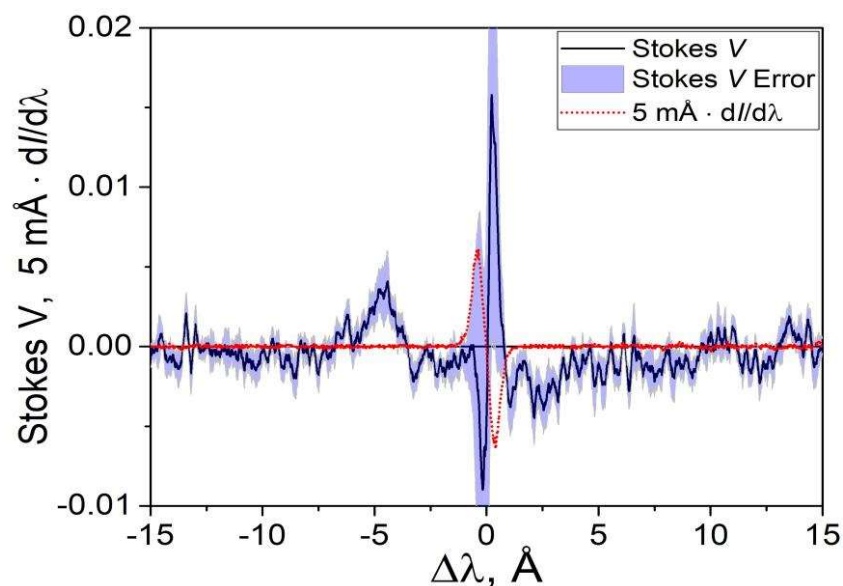
Figure 5. Stokes V profile of the D3 line in limb flare of June 10, 2014, averaged over a height interval of 4 Mm. For comparison, the profile of the parameter $dI/d\lambda$ is shown with a red curve.
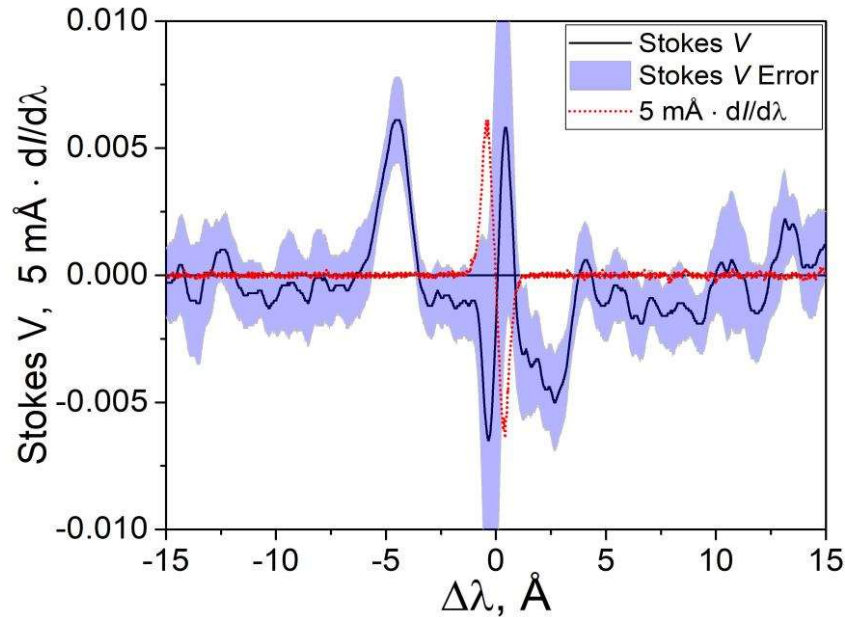
Figure 6. The same as in Fig. 5, but for averaging height range of 7 Mm, from 2 to 8 Mm. Additional smoothing with a sliding window of 770 mÅ was also applied.

Thus, the consideration in the presented study of a wider spectral interval of ±15 Å instead of ±2.5 Å as in the work of Yakovkin & Lozitsky (2022) turned out to be quite justified from a methodological point of view: if only this narrower interval were considered again, the above-mentioned features on $\Delta\lambda$ = -4.5 Å and +2.7 Å could be omitted. This indicates that further searches for extremely strong magnetic fields on the Sun should be conducted precisely in an extended range of wavelengths – perhaps even wider than ±15 Å. This can be problematic if using a Fabry-Perot filter rather than a diffraction spectrograph.

In general, the general picture of the magnetic field in this limb flare is as follows: against the background of the sub-kilogauss magnetic field (400-600 G) of *S* polarity, there were probably also extremely strong (~10^5 G) small-scale magnetic fields of the opposite (*N*) polarity, in which there were relatively high Doppler velocities. It is also possible that there was a significant dispersion of the magnetic field in the small-scale component. This can be indicated by the fact that the width of the peaks at $\Delta\lambda$ = -4.5 Å and +2.7 Å is quite significant, 1.4-1.7 Å, which is several times larger than the theoretical width of the σ components of the D3 line in the case of a uniform magnetic field (see Section 4 below).

4. THEORETICAL EFFECTS IN SPLITTING OF D3 LINE

In order to further assess the possibilities for 100 kG fields to exist in prominences we have conducted a numeric simulation of He I D3 spectral line profiles using the HAZEL code by Asensio Ramos, Trujillo Bueno and Landi Degl'Innocenti (2008). The code was created for synthesis and decoding of the Stokes profiles for atoms in magnetic fields, accounting for Hanle and Zeeman effects. Since Hanle effect is observed only for weak magnetic fields, the synthesis was accounting for Zeeman effect and fine structure splitting in terms of atomic term structure.

According to calculations, the D3 line splits at magnetic fields in the range of 500-2000 G so that the displacement of the "centers of gravity" of the $I \pm V$ profiles as a whole resembles the classic case of linear splitting at weak fields, assuming that its Lande factor g_{eff} = 0.94. The corresponding calibration formula (2) is given above in section 3. The second characteristic feature of the line splitting in this field range is that the entire splitting pattern has a *red shift* of about 0.02 Å (Fig 7).
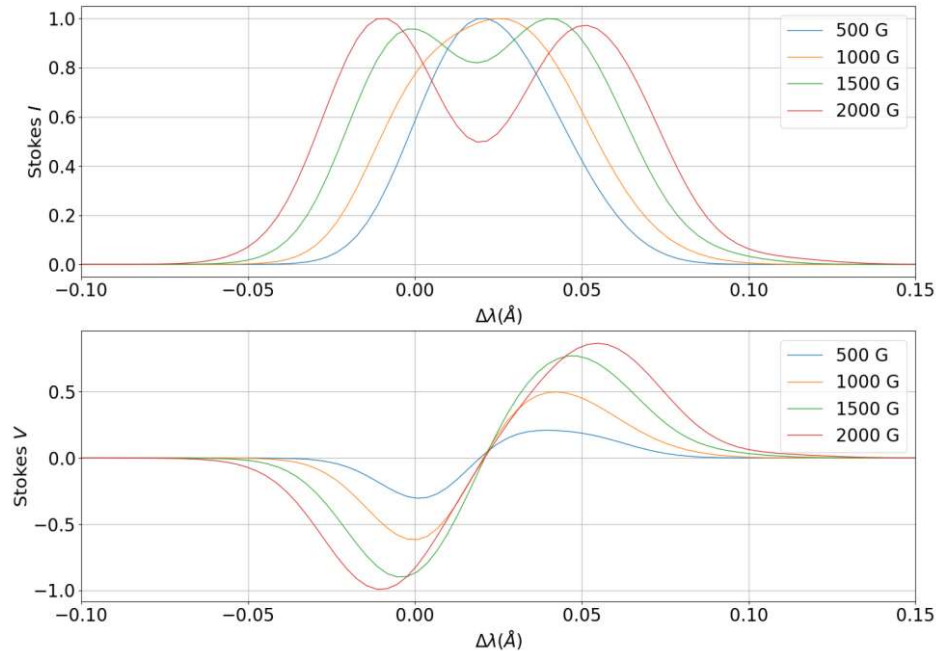
Figure 7. Theoretical Stokes *I* (upper panel) and *V* (lower panel) profiles of the D3 line for magnetic fields of 500, 1000, 1500, and 2000 G.

It should be noted that the HAZEL code can account for arbitrary magnetic field strengths, enabling accurate interpretations across all cases of magnetic field strength, from linear Zeeman splitting (LZS) to complete Paschen-Back effect, as well as intermediate fields (incomplete Paschen-Back effect, see Socas-Navarro et al., 2004). Therefore, we can employ the HAZEL code to search for interpretations of the observed profiles in all ranges of magnetic fields.

Figs. 8 and 9 show the typical Stokes *I* and *V* profiles of He I D3 spectral line for different values of the magnetic field strength. Notably, the typical width of the He I D3 line due to fine structure is in the range of 0.2-0.3 Å for arbitrary values of magnetic fields. Therefore, we can conclude that the observed line profiles at extremely strong magnetic fields should either have a pronounced fine structure or be at least around 0.3 Å wide. While the spectral term structure of the He I atom is dictated by the value of the applied magnetic field, the broadening of the He I D3 spectral line is defined also by the macroscopic parameters of the prominence: temperature, turbulent velocities, optical thickness etc.

The set of macroscopic parameters can be chosen differently depending on the available information about the investigated phenomenon. The simplest and straightforward way is by using a single parameter: temperature. Then the width of the observed line is interpreted as caused by temperature broadening. This approach is suitable for very rough estimations for

narrow spectral profiles, but the analysis of the events in multiple spectral lines shows that a single macroscopic parameter is not nearly sufficient for consistent quantitative results. In order to make the measurements of macroscopic parameters consistent typically a set of at least 3-4 macroscopic parameters is needed, a typical choice being the temperature, turbulent velocity and optical width.
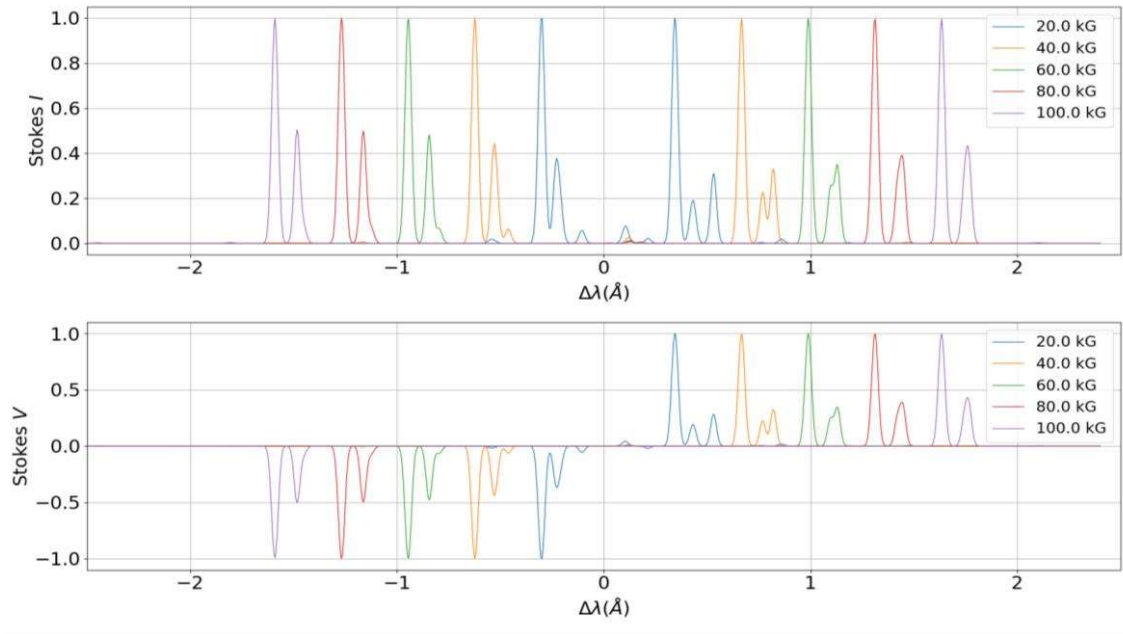
Figure 8. Sample He I D3 line profiles *I* (above) and *V* (below) for different values of magnetic fields and for optical depth $\tau = 0.1$.
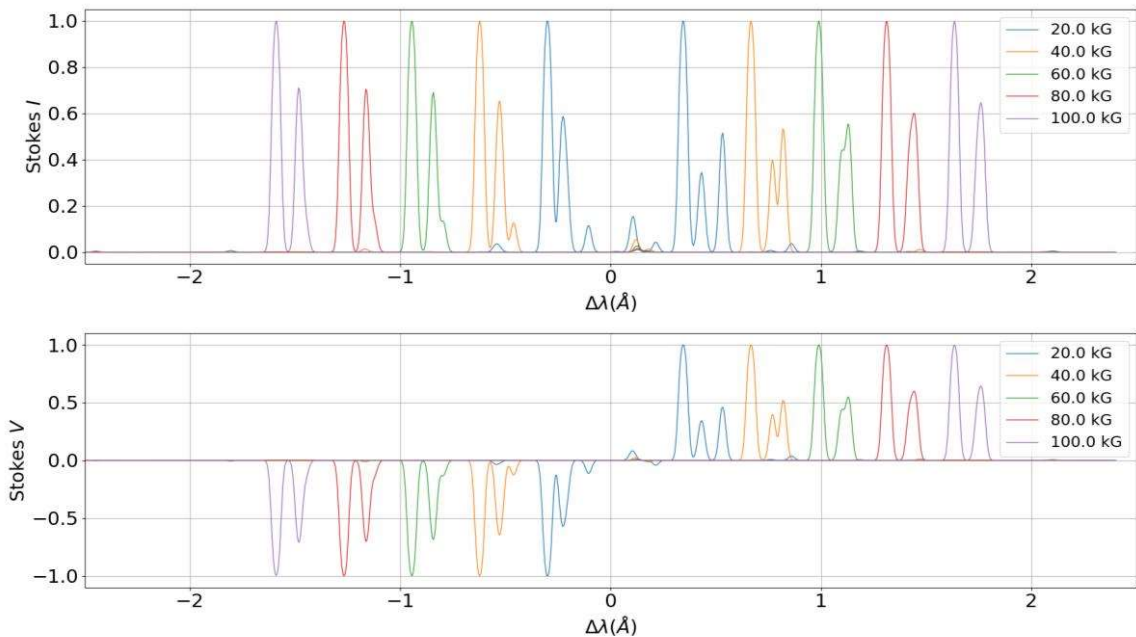
Figure 9. The same as in Fig. 8 but for optical depth $\tau = 1.0$.

An alternative or complementary technique regarding the turbulent velocity is modelling multiple emission components. Accounting for multiple emission components is often necessary when the spectrum shows multiple discreet Doppler-shifted emission peaks (Yakovkin et al, 2021). If there is only one emission peak, modelling it using a large number of emission components can be a much more flexible and general alternative to introducing the turbulent velocity.

The need to use multi-component model can be spotted by analysing the Stokes I and $I \pm V$ profiles. If the Stokes I profile has multiple peaks which are not the result of the Zeeman or fine structure splitting, multiple components are necessary to properly synthesise the profiles. Similar criterium can be made using the Stokes $I \pm V$ profiles or the corresponding bisector shifts: if the splitting between $I + V$ and $I - V$ profiles is significantly non-constant then it is an indicator of multiple emission components. When studying active events of the Sun accounting for multiple emission components is almost always necessary due to the physical nature of such events: the matter is under constant complex and seemingly chaotic motion which in terms results in complex spectral line profiles. Therefore, it is absolutely necessary to either simulate all bursts of plasma as separate components, or at least to introduce a rough model of plasma motion (e.g., turbulent velocity model) to correctly interpret the observed spectral data.

HAZEL program allows for a very broad set of parameters to describe the emission formed in the solar atmosphere, most important of which are optical density, macroscopic speed, enhancement factor, Voigt profile damping, and magnetic field vector. HAZEL allows for simulation of multiple atmospheres (i.e., different volumes with different parameters, or an in-place superposition of atmospheres with by introducing the filling factors). From general analysis of our observed spectral profiles, it is apparent that the model should account for several independent emission components. This can be easily implemented using the HAZEL code, but accounting for multiple emission components means effectively multiplying the number of fitting parameters. Such high number of parameters (around 30 in case of 3 components), complemented by different ways to position the emissive volumes, as one can expect, results in either overfitting (unrealistic values of parameters in attempt to fit the smallest noise-related irregularities) or redundancy (the same profile can be achieved by multiple sets of parameter values). Therefore, to avoid any ambiguities, in the current research we do not use HAZEL to directly determine the exact values of the physical parameters of the event. Instead, we focus on the following questions:

1. Can the presented observed spectral profiles be obtained using realistic macroscopic parameters accounting for our estimates of magnetic field strength?

2. Can such profiles be obtained using significantly weaker magnetic fields?

The answers to these questions were obtained by modeling line profiles.

5. RESULTS OF MODELING

The simulation was performed for a three-component model, as it was deemed optimal for the spectral analysis. Utilizing fewer components would have been too restrictive, while adding more components did not significantly improve the qualitative fit. Two different scenarios were

investigated: one with a super-strong magnetic field to assess the possibility to explain such profiles with superstrong fields, and the other with lower magnetic field values.

The first scenario involved a super-strong magnetic field calculation, which corresponds to the parameters in model A, as presented in Table 1. In this Table, B_x is magnetic field strength (in gauss) assuming that field lines are parallel to line of sight (case of pure longitudinal field), τ is the optical depth, v_{mac} is the macroscopic speed (in km s^{-1}), v_{Doppl} is Doppler velocity (in km s^{-1}), β is the enhancement factor, a is damping constant, ff is filling factor. Figure 10 presents a comparison between the observed spectral profiles of the D3 spectral line in the active prominence observed on July 12, 2004 at a height of 21 Mm, and the simulated profiles generated using these parameters.

Table 1. Parameters of model A which gives line profiles presented in Fig. 10

Parameter	First component	Second component	Third component
B_x	0	0	104000
τ	0.2	0.2	0.2
v_{mac}	0.3	-6	-3.9
v_{Doppl}	24	50	16
β	1	1	1
a	0.05	0.1	0
ff	0.83	0.16	0.01
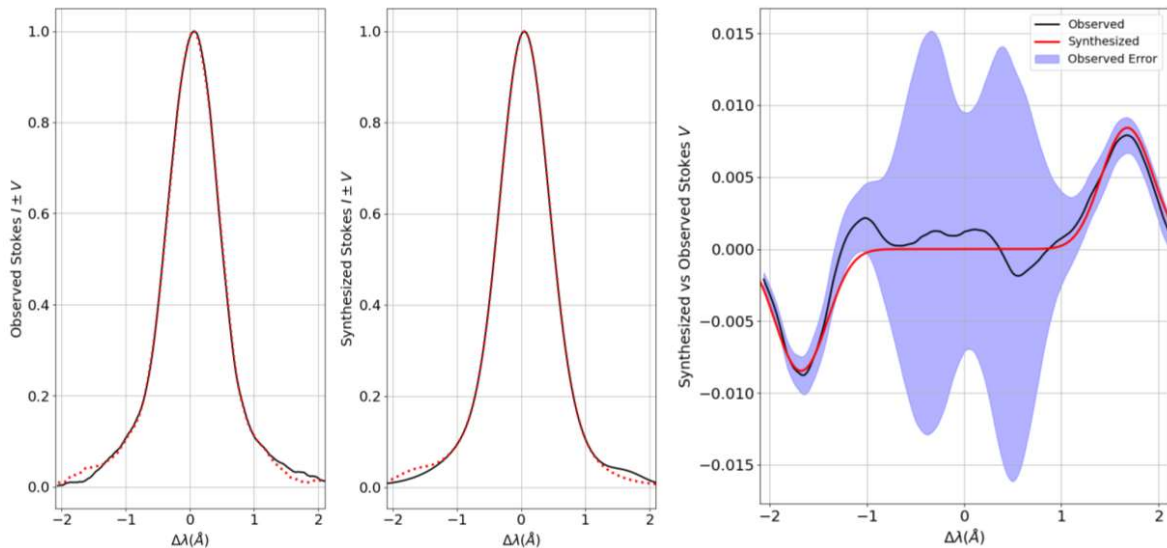
Figure 10. Comparison of the synthesized using the Model A and the observed He I D3 Stokes $I \pm V$ and V profiles of the July 12, 2004 active prominence at 21 Mm above the photosphere.

As can be seen from the graduation of the abscissa axis in the graphs, we limited ourselves only to the range of wavelengths ± 2.2 Å, that is, we do not consider those subtle effects that correspond to a wider range of distances from the center of the line and are presented above in

Fig. 4. Regarding Fig. 10, then on it the left panel represents the $I \pm V$ profiles in model A, and the middle panel represents the similar observed profiles. The right panel of this Figure shows the Stokes V profiles, with the dotted line showing the observed profiles and the solid red line showing the model calculation. The synthesized $I \pm V$ and V profiles match well with the observed ones, and the values of the 3-component model parameters are in good agreement with previously made estimates from direct measures of the magnetic splitting. However, the gigantic magnitude of the magnetic field (104 kG) in this model is alarming.

To address this concern, an alternative scenario was considered, which utilized the superposition of highly Doppler-shifted (± 50 km/s) components with lower magnetic field values. Figure 1 further confirms the presence of such components, as it clearly demonstrates their existence at altitudes of 3-15 Mm, thus making their presence at 21 Mm highly likely. The corresponding parameters for this scenario can be found in Table 2, and the associated line profiles are presented in Figure 11.

Table 2. Parameters of model B which gives line profiles presented in Fig. 11

Parameter	First component	Second component	Third component
B_x (G)	230	7100	5580
τ	0.2	0.2	0.2
v_{mac} (km/s)	-0.1	-58.9	51.3
v_{Doppl} (km/s)	25	41	31
β	1	1	1
a	0.08	0.12	0.0
ff	0.91	0.05	0.04
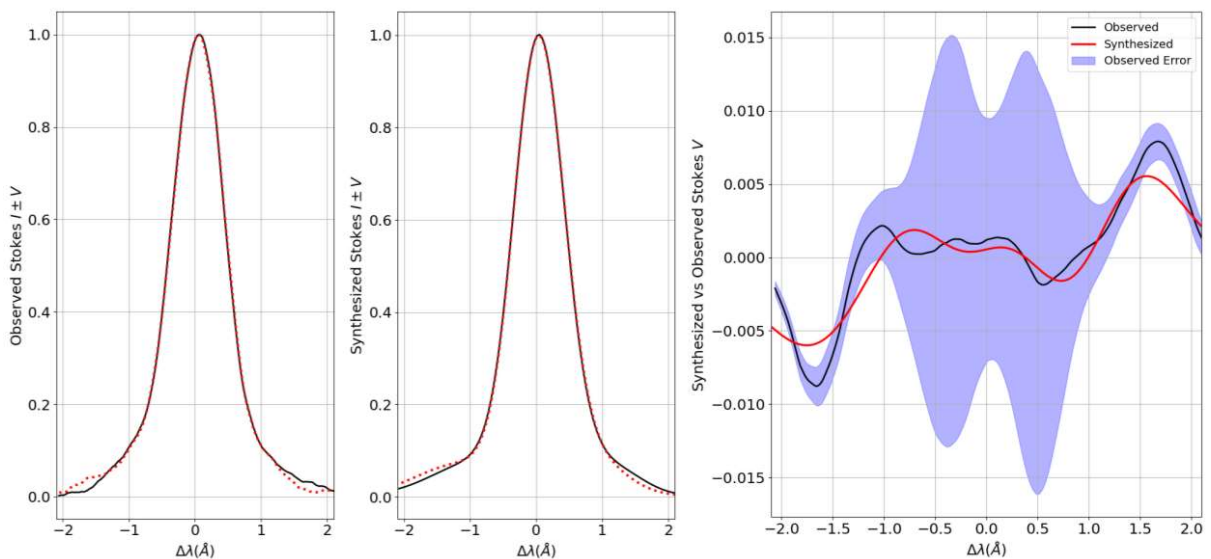
Figure 11. Same as in Fig. 9, but for model B, which accounts for highly shifted components.

The weaker-field simulation, considering the superposition of highly Doppler-shifted components with lower magnetic field values, has similar fitting quality compared to the strong-field simulation. Moreover, the quality could be easily improved by adding more components. Different combinations of magnetic field polarities and Doppler shifts were tested, and the presented weak-field scenario yielded the best results. Overall, the approach considering the highly-shifted components appears to be more promising and provides a better explanation for the observed spectral profiles.

Thus, we conclude that the weak-field scenario is more likely to be the case for the presented observations, although further investigation into this approach is still warranted.

DISCUSSION

In the case of our observations, the instrumental polarization (IP) may have some influence on the line profiles. This issue was addressed in our previous paper by Yakovkin & Lozitsky (2022) and noted that for magnetic field measurements by $I + V$ and $I - V$ profiles, the essential influence of IP occurs due to the linear-to-circular transformation effect (LCT-effect). If linear polarization is zero, the observed $I + V$ and $I - V$ profiles are not distorted by IP. In this case, we can expect an insignificant role of IP for observations of magnetic features with almost longitudinal field ($\gamma = 0°$ or $180°$).

In the strong field regime, the instrumental polarization distorts only the amplitude of the secondary peaks of the Stokes V parameter, but not their location relative to the line center. But it is the splitting of the oppositely polarized secondary peaks that allows us to estimate the magnitude of the magnetic field. In this study, we did not aim to accurately account for the instrumental polarization by obtaining the Mueller matrices. We were just trying to understand the nature of the detected effects, i.e. they are solar or instrumental effects. As for the instrumental polarization, it depends on the angles of oblique incidence of the rays on the astronomical mirrors as well as the diffraction grating. It was found that with practically the same (with great accuracy) angles of incidence, we have very different amplitudes of the secondary peaks of the V parameter in different locations of the prominence and the solar flare. This convinces us that it is a solar effect after all. From our data it follows that this effect reflects not only magnetic fields, but also significant Doppler shifts.

It should also be taken into account that currently observational indications of magnetic fields at the level of 10^4-10^5 G have been found at different levels of the solar atmosphere - from the photosphere to the lower solar corona. Perhaps the most convincing are the data obtained in Fe I lines with very low Lande factors, about 0.01 in absolute value, determined in laboratory conditions (Lozitsky, 1993, 2009). Such data relate to solar flares and the height range "upper photosphere - lower chromosphere" (0.4-0.6 Mm), where the emission peaks of the Fe I 5434.5 line are formed, for which the Lande factor is $g_{eff} = - 0.014$. This line reveals signs of Zeeman splitting in some sunspot locations too, which may indicate superstrong magnetic fields of the same range (Lozitsky et al., 2022). In the latest work, its authors tried to find relevant evidence from data in unpolarized light, that is, in the Stokes I parameter, taking into account that such extremely strong fields can be sub-telescopically "entangled" and not produce effects in polarized light. It turned out that two lines of the 15th multiplet of iron, Fe I 5397.1 and 5434.5

Å, which have almost the same temperature sensitivity and height of formation in the Sun's atmosphere, behave very differently during the transition from the photosphere to the sunspot. The behavior of the Fe I 5397.1 Å line is quite understandable and typical for this case, while the Fe I 5434.5 Å line reveals separate places with an additional broadening of its profile by $\approx$ 10%, which is very difficult to explain by thermodynamic effects and variations of the velocity field. Regarding the possible effect of spectral blends, the paradox is that the line (Fe I 5434.5 Å) that is more spectrally "pure" than the line that is more blended (Fe I 5397.1 Å) shows such unclear effects. If the above additional expansion is due to the magnetic field, then its value should be $\sim$ 10^5 G. Naturally, if such extremely strong magnetic fields really exist, then they should give corresponding spectral manifestations also in spectral lines with larger Lande factors, for example, close to unity. As mentioned above, such spectral manifestations were recently found in a limb solar flare (Yakovkin & Lozitsky, 2022).

It is hard to believe in the existence of such fantastic magnetic fields because they must be some very unusual fields, significantly different from the well-known magnetic fields in sunspots. For sunspots, the situation is more transparent and understandable, since the observations there can be explained by the simplest model with an untwisted power tube, for which the balance of two pressures is performed: the magnetic pressure inside the power tube and the external gas pressure outside this tube. Theoretically, this gives a magnetic field of $\sim10^3$ G - exactly the same range that is noted by observations. However, for magnetic fields of the level of 10^5 G localized in the chromosphere and especially in the lower corona, this interpretation is not applicable, since the magnetic pressure in the corresponding structures is $\sim10^8$ dyn cm^{-2}, i.e. several orders of magnitude greater than the pressure of the external plasma (in the corona and chromosphere this pressure in the range of $10^{-1} \div 10^2$ dyn cm^{-2}). That is, simple untwisted power tubes with such fields cannot exist there, but there can only be some more complex configurations, for example, with strongly twisted power lines. It is possible, in particular, that these are configurations of exactly the type proposed recently by Solov'ev (2022). However, in order to be sure of this, and at the same time, of the reality of such extremely strong magnetic fields, it is necessary to make sure step by step that the theoretical parameters correspond to the observed data. At the moment, we can only state that the estimates of the magnetic field strengths in the above-mentioned theoretical work are close to those derived from our observational data. The low filling factor of the super-strong component according to observational data, about 1% (Table 1), is also qualitatively consistent with the theoretical picture of the lateral distribution of the field presented in Fig. 5 in paper by Solov'ev (2022). In addition, observational data suggest that volumes with super-strong fields should have a low macroscopic velocity, as well as a reduced Doppler velocity. The last two features are characteristic not only for the studied prominence, but also for solar flares, in which somewhat weaker magnetic fields of the 10^4 G level were found (Lozitsky, 2015). Based on the published data, it is not yet clear how unambiguously these features follow from theoretical models.

CONCLUSION

The main conclusion of our work is that the observed data allow for two tentative interpretations: (a) the possible existence of particularly strong magnetic fields in the 10^5 G range and (b) the

presence of weaker magnetic fields of the "kilogauss" level (5.5-7.1 kG) in the investigated active processes, which correspond to areas with relatively fast movements (50-60 km per second) of both signs. Clearly, to explain their existence, some very original and well-founded theoretical model is needed. This model should also take into account the following approximate features of ultra-strong magnetic fields: (a) a significant dispersion of magnetic field strengths, which is visible from the width of the secondary peaks of the V parameter and (b) a significant dispersion of radial velocities - from zero to several tens of km s^{-1}, and, possibly, even more. Another feature emerges from our observations: such extremely strong magnetic fields can be observed relatively often, and with low spatial resolution and not very high spectral resolution. Much more important in this regard is a high signal-to-noise ratio. The width of the registration spectral interval is also important - it should be at least ±15 Å, and preferably even more. Apparently, this can be problematic for spectropolarimeters based on Fabry-Perot filters, but is quite possible for diffraction spectrographs. In general, above-mentioned features are in agreement with similar super-strong magnetic fields manifestations reported previously by Lozitsky (1993, 2015) and Yakovkin & Lozitsky (2022).

DATA AVAILABILITY

The original contribution presented in the study are included in the article.

ACKNOWLEDGEMENTS

REFERENCES

Asensio Ramos, A., Trujillo Bueno, J., Landi Degl'Innocenti, E. 2008, ApJ, 683, 542
Bruce C.E.R., 1966, Observatory. 86, 82
Cauzzi G. et al., 1993, Solar Phys. 146, 207
Durán C.J.S. et al., 2020, ApJ, 895:129, 18pp
Frish S.E., 2010, Optical atom spectra. St.-Peterburg. Moscow. Krasnodar, 656 p.
Gordovskyy M., Lozitsky V.G., 2014, Solar Phys., 289, 3681
Harvey J.W., 2012, Solar Phys., 280, 69
Jefferies J.T., Mickey D.L., 1991, Ap J, 372, 694
Kirichek E.A. et al., 2013, Geomagn. & Aeronomy. 53, 831
Kleint L., 2017, ApJ, 834, art. id. 26, 10 pp.
Libbrecht T. et al., 2019, Astron. Astrophys, 621, id. A35, 21 pp.
Livingston W., Harvey J.W., Malanushenko O.V., 2006, Solar Phys., 239, 41
Lozitsky V. et al., 2022, ApJ, 928, Iss. 1, id.41, 7 pp.
Lozitsky V. G., 2016, Adv. Space Res., 57, 398
Lozitsky V. G., Osipov S. M., Stodilka M. I., 2022, J. Phys. Studies, 26, No. 4, id. 4902, 14 pp.
Lozitsky V.G. et al., 2000, Solar Phys.,191, 171
Lozitsky V.G., 1993, Kinematics and Physics of Celestial Bodies. 9, 18
Lozitsky V.G., 2009, Journal of Physical Studies. 13(2), 2903-1

Lozitsky V.G., 2015, Adv. Space Res., 55, 958

Moore Ch.E, et al., 1966, The solar spectrum 2935 Å to 8770 Å. Second revision of Rowland's Preliminary Table of solar spectrum wavelengths. National Bureau of Standards, Monograph 61, Washington, 349p

Sasikumar Raja et al., 2022, Adv. Space Res. 69, 814

Severny A.B., 1957, Astronomicheskii Zhurnal, 34, 684

Socas-Navarro H. et al., 2004, ApJ, 612, 1175

Solanki S.K., 2003, Astron. Astroph. Rev. 11, 153

Solov'ev A.A., 2022, MNRAS, 515, 4981

Van Noort M. et al., 2013, Astron. Astrophys., 557, id. A24, 14 pp

Wang H. et al., 2018, Res. Notes of the Amer. Astron. Society, 2, No. 1

Wei Yudian et al., 2021, ApJ, 923, 213

Yakovkin I.I. et al., 2021, Adv. Space Res. 68, 1507

Yakovkin I.I., Lozitsky V.G., 2022, Adv. Space Res. 69, 4408

This paper was prepared by the authors in Word